

# Berry-phase effects and electronic dynamics in noncollinear antiferromagnetic texture

Olena Gomonay

*National Technical University of Ukraine “KPI”*

*ave Peremogy, 37, 03056, Kyiv, Ukraine*

## Abstract

Antiferromagnets (AFMs), in contrast to ferromagnets, show a nontrivial magnetic structure with zero net magnetization. However, they share a number of spintronic effects with ferromagnets, including spin-pumping and spin transfer torques. Both phenomena stem from the coupled dynamics of free carriers and localized magnetic moments. In the present paper I study the adiabatic dynamics of a spin-polarized electrons in a metallic AFM exhibiting a noncollinear  $120^\circ$  magnetic structure. I show that the slowly varying AFM spin texture produces a non-Abelian gauge potential related to the time/space gradients of the Néel vectors. Corresponding emergent electric and magnetic fields induce rotation of spin and influence the orbital dynamics of free electrons. I discuss both the possibility of a topological spin Hall effect in the vicinity of topological AFM solitons with nonzero curvature and rotation of the electron spin traveling through the AFM domain wall.

PACS numbers: 75.50.Ee 85.75.-d

Keywords: Antiferromagnet, Berry phase, spintronics

## I. INTRODUCTION

Metallic and semiconducting antiferromagnets (AFM) with high ordering (Néel) temperature are promising candidates for spintronic applications. Compared to their ferromagnetic counterparts, AFM-based devices show reduced critical currents for magnetization switching<sup>1</sup> and can effectively operate at higher frequencies.<sup>2</sup> According to theoretical predictions, AFMs can also show the following current-induced phenomena typical for ferromagnets: spin-transfer torques,<sup>3-5</sup> spin pumping<sup>6</sup>, domain wall motion<sup>7,8</sup>, – but with much richer physics stemming from the nontrivial magnetic structure.

However, the mechanisms responsible for the coupled dynamics of free electrons and localized magnetic moments in AFMs are still not clear and thus recently became a matter of interest. For example, ferromagnets can work as spin polarizers due to exchange coupling between the localized spins (that contribute to macroscopic magnetization) and the spin of the conduction electron. In contrast, the AFMs have zero or vanishingly small magnetization. The symmetry properties of the Néel vector (AFM order parameter) differ from those of the spin vector and thus the polarization mechanism through  $sd$ -exchange is excluded. On the other hand, AFMs have a nontrivial magnetic structure which removes degeneracy of otherwise equivalent directions and/or planes and thus can affect spin dynamics of free electron. The nontrivial spintronic effects in AFMs are usually attributed to  $sd$ -exchange and/or spin-orbit coupling. In homogeneous systems the spin-orbit interaction can induce polarization of the electric current which flows through the collinear AFM<sup>9</sup> or the anomalous Hall effect in noncollinear planar AFM.<sup>10,11</sup> Exchange interaction itself can induce the topological Hall effect in the structure with the nonzero chirality<sup>12,13</sup>, e.g. in non-coplanar AFMs.<sup>14,15</sup>

The  $sd$ -exchange also plays an important role in the magnetic textures which can produce Abelian<sup>16</sup> and non-Abelian<sup>17</sup> gauge potentials for conduction electrons. Corresponding fields contribute to adiabatic spin-transfer torque and spin-pumping phenomena and thus could be experimentally detected. In particular, a *ferromagnetic* texture produces an effective spin-dependent  $U(1)$  gauge field for conduction electrons. This gauge field gives rise to effective electrical and magnetic fields proportional to the macroscopic magnetization of the ferromagnet. An alternative point of view relates the emergent fields with the Berry phase accumulated by a free electron whose spin is aligned with the local macroscopic

magnetization.<sup>18</sup> An analogous influence of the collinear *antiferromagnetic* texture on the dynamics of free carriers was recently predicted in Ref. 17 from semiclassical analysis of Berry phase. The Berry phase also strongly affects the semiclassical motion of electrons in chiral magnets with spin-orbit interaction and can even induce formation of skyrmions in these materials (“driving force for formation”), as was recently demonstrated in Ref. 19.

The present paper focuses on the dynamics of spin-polarized electrons in the gauge potentials produced by the space/time varying magnetic moments of a noncollinear AFM. The main idea is to demonstrate that the adiabatic dynamics of free electrons is intimately related to the “dynamic” magnetization of AFM (no matter how complicated AFM structure is) and in this sense is similar to adiabatic dynamics of transport electrons in ferromagnets. Correspondingly, the curvature of a smooth distribution of AFM vectors generates effective electric and magnetic fields that affect, via *sd*-exchange coupling, the orbital motion of free electrons. I predict a possibility of topological spin Hall effect in noncollinear AFM textures that, in analogy with its ferromagnetic counterpart, originates from the *sd*-exchange. This effect can be used to generate spin-currents and probe the curvature of the AFM distribution. I demonstrate that an inhomogeneous AFM structure induces a rotation of the spin polarization (analog of Faraday effect). This effect can be an efficient tool for probing the AFM domain structure by electrical methods.

## II. MODEL AND FORMALISM

As a prototype of a conductive antiferromagnet with noncollinear magnetic structure I consider the antiperovskite  $\text{Mn}_3\text{XN}$  ( $\text{X}=\text{Ag}, \text{Zn}, \text{Ni}, \text{Ga}$ ) with cubic space group  $\text{Pm}\bar{3}\text{m}$  (see Fig.1) and with the magnetic moments localized at Mn atoms.<sup>20</sup> Although some authors<sup>21-23</sup> underline that strong hybridization around the Fermi level points to the itinerant nature of antiferromagnetism in Mn-based antiperovskites, these substances could be effectively described by the Néel model of magnetic sublattices.<sup>24-26</sup>

The Mn-based perovskites combine the nontrivial triangular magnetic structure with the peculiar transport properties. The linear temperature dependence of the resistivity and strong hybridization of Mn-3*d* and N-2*p* electrons around the Fermi level<sup>22</sup> suggests a metallic character of conductivity. However, conductivity and temperature coefficient of resistivity are much smaller than those of a typical metal.<sup>27,28</sup> Hence, these compounds could be con-

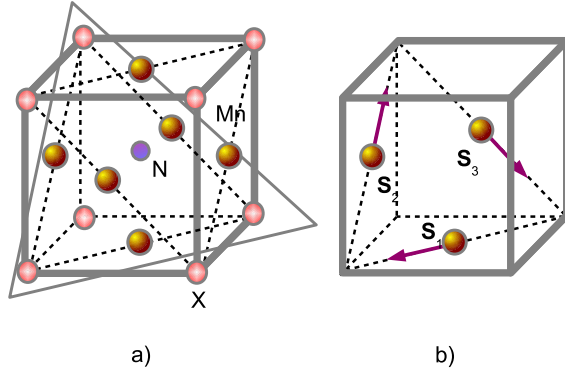


Figure 1. (Color online) Unit cell (a) and  $\Gamma^{5g}$  magnetic structure (b) of antiperovskite  $\text{Mn}_3\text{XN}$ . Magnetic moments  $\mathbf{S}_1$ ,  $\mathbf{S}_2$  and  $\mathbf{S}_3$  are localized at Mn atoms.

sidered as bad metals with hopping character of conductivity. Resistivity measurements<sup>28</sup> also indicate to a strong coupling between the magnetic structure and the transport properties. In addition, suppressed  $sd$  scattering in the magnetic phase<sup>28</sup> enables observation of the quantum phase effects. Thus,  $\text{Mn}_3\text{XN}$  compounds are generic materials for analysis of the Berry-phase effects in noncollinear AFMs.

### A. Magnetic structure formed by localized moments

The localized magnetic moments (sublattice magnetizations) represented by three classical vectors  $\mathbf{S}_j$ ,  $j = 1, 2, 3$  form a non-collinear coplanar structure classified<sup>29</sup>, depending on the material, as  $\Gamma^{5g}$  or  $\Gamma^{4g}$ .<sup>20</sup> Vectors  $\mathbf{S}_j$  make  $120^\circ$  angle with respect to each other. Thus, the total magnetization cancels within the plane. The ordering plane is defined by the plane normal  $\mathbf{n}$ . Well below the Néel temperature  $|\mathbf{S}_j| = S$ .

Within the macroscopic approach a noncollinear AFM structure can be conveniently described by two mutually orthogonal AFM, or Néel, vectors  $\mathbf{L}_1 \perp \mathbf{L}_2$  ( $|\mathbf{L}_1| = |\mathbf{L}_2| = S$ ) that could be considered as a multicomponent order parameter:

$$\mathbf{L}_1 = \frac{1}{\sqrt{6}} (2\mathbf{S}_1 - \mathbf{S}_2 - \mathbf{S}_3), \mathbf{L}_2 = \frac{1}{\sqrt{2}} (\mathbf{S}_2 - \mathbf{S}_3), \quad (1)$$

and the macroscopic magnetization vector

$$\mathbf{M} = \frac{1}{\sqrt{3}} (\mathbf{S}_1 + \mathbf{S}_2 + \mathbf{S}_3). \quad (2)$$

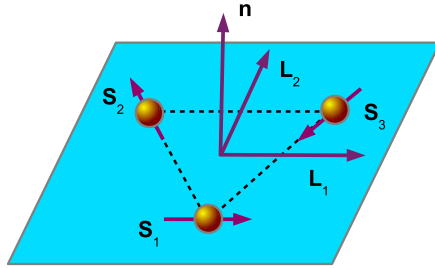


Figure 2. (Color online) Local frame generated by AFM vectors  $\mathbf{L}_1$ ,  $\mathbf{L}_2$ , and vector  $\mathbf{n}$  normal to the plane of spin ordering.

From the symmetry point of view vectors (1) and (2) belong to different irreducible representations of the permutation group  $P_3$  (corresponding to the exchange symmetry of the crystal).<sup>24</sup>

In the AFM ground state the macroscopic magnetization  $\mathbf{M} = 0$ . Three orthogonal vectors  $\mathbf{L}_1 \perp \mathbf{L}_2 \perp \mathbf{n}$  generate a natural local frame for free spin (see Fig.2).

In equilibrium homogeneous state the corresponding vectors are  $\mathbf{n}^{(0)} \parallel [111]$ ,  $\mathbf{L}_1^{(0)} \parallel [0\bar{1}1]$ , and  $\mathbf{L}_2^{(0)} \parallel [2\bar{1}\bar{1}]$ . In the texture (inhomogeneous state) the orientation of the sublattice magnetizations can smoothly vary at the length-scale much greater than interatomic distances, thus, all the magnetic vectors  $\mathbf{S}_j$ ,  $\mathbf{L}_1$ ,  $\mathbf{L}_2(t, \mathbf{r})$  are continuous functions of time and space.

Strong exchange coupling locks the mutual orientation of localized moments even in the presence of relatively small external fields. However, under the action of these fields the whole structure can smoothly rotate with respect to some initial configuration (labeled further with the subscript (0)). In the adiabatic approximation which we consider below, the large scale variation of localized moments is equivalent to solid-like rotation of vectors  $\mathbf{S}_j$  (and, correspondingly,  $\mathbf{L}_1, \mathbf{L}_2, \mathbf{n}$ ) and can be conveniently parametrized<sup>30,31</sup> with the Gibbs' vector  $\varphi$  (so-called Cayley-Gibbs-Rodrigues parametrization) as follows:

$$\mathbf{S}_j = \mathfrak{R}(\varphi) \mathbf{S}_j^{(0)} \equiv \frac{1 - \varphi^2}{1 + \varphi^2} \mathbf{S}_j^{(0)} + \frac{2}{1 + \varphi^2} \left[ \varphi \times \mathbf{S}_j^{(0)} + \varphi (\varphi \cdot \mathbf{S}_j^{(0)}) \right]. \quad (3)$$

Here  $\mathfrak{R}(\varphi)$  is the orthogonal rotation tensor,  $\varphi(t, \mathbf{r}) \equiv \tan(\theta/2) \mathbf{N}$ , where  $\mathbf{N}(t, \mathbf{r})$  is the instant rotation axis,  $\theta(t, \mathbf{r})$  is the rotation angle and we treat all the parameters as

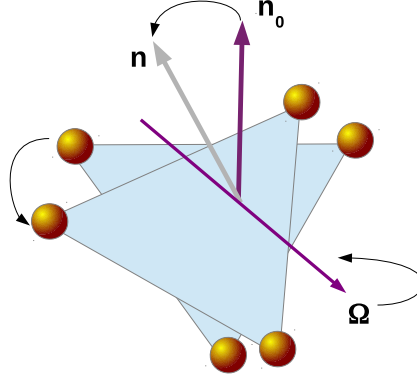


Figure 3. (Color online) Solid-like rotation of the magnetic structure. Angular velocity  $\Omega$  may result either from the time or space rotation of the AFM structure, as described in the text.

continuous functions of space and time.

Rotation of AFM moments plays an important role in the magnetic dynamics of localized spin. As it was pointed out by Andreev and Marchenko,<sup>30</sup> a solid-like rotation of spins induces nonzero, “dynamic” magnetization of AFM,  $\mathbf{M}_{dyn} \propto \hat{\chi} \Omega_t$  ( $\hat{\chi}$  is a tensor of magnetic susceptibility), which is proportional to the pseudovector  $\Omega_t$  of angular velocity, frequently referred to as macroscopic spin (see Fig.3):

$$\Omega_t = 2 \frac{\partial_t \varphi + \varphi \times \partial_t \varphi}{1 + \varphi^2}, \quad \partial_t \mathfrak{R}(\varphi) = \Omega_t \times \mathfrak{R}(\varphi). \quad (4)$$

However, a free electron moving with velocity  $\dot{r}_l$  ( $l = x, y, z$ ) in the slowly varying AFM texture should also “feel” the effective magnetization produced by space rotations of the AFM moments and described by the “space” angular velocity:

$$\Omega_l = 2 \frac{\partial_l \varphi + \varphi \times \partial_l \varphi}{1 + \varphi^2}, \quad \partial_l \mathfrak{R}(\varphi) = \Omega_l \times \mathfrak{R}(\varphi). \quad (5)$$

Thus, in the continuous medium the dynamic magnetization of AFM seen by conduction electron is proportional to the angular velocity  $\Omega = \Omega_t + \Omega_l \dot{r}_l$ .

In what follows we consider the functions  $\varphi(t, \mathbf{r})$ ,  $\Omega(t, \mathbf{r})$  that describe the AFM texture as given, putting aside the problem of current-induced dynamics of localized spins.

## B. Effective Hamiltonian and band structure

The transport properties of the system are described within the nearest-neighbor tight-bonding approximation validated by low carrier density<sup>27</sup> and high resistivity<sup>32</sup> of Mn-based antiperovskites. In our toy model we consider only those electrons that hop between Mn sites as they give the main contribution to the transport properties.<sup>21,22,28</sup> Then the local Hamiltonian for the conduction electrons takes a form:

$$\hat{H}(\mathbf{r}, t) = \sum_{j\tau} \varepsilon_0(\mathbf{k}) \hat{a}_{j\tau}^\dagger \hat{a}_{j\tau} + \sum_{j,l,\tau} \gamma_{jl}(\mathbf{k}) \hat{a}_{j\tau}^\dagger \hat{a}_{l\tau} - J_{sd} \sum_{j\tau,\tau'} \mathbf{S}_j(t, \mathbf{r}) \hat{a}_{j\tau}^\dagger \hat{\sigma}_{\tau\tau'} \hat{a}_{j\tau'}, \quad (6)$$

where the first term in the r.h.s. describes the kinetic energy related with the crystal translational symmetry. Fermi-operators  $\hat{a}_{j\tau}$  and  $\hat{a}_{j\tau}^\dagger$  describe annihilation/creation of the electrons with the Bloch functions  $|u_j\rangle$  ( $\langle u_k | u_j \rangle = \delta_{kj}$ ) and in the spin states  $|\tau\rangle$  ( $\tau = \uparrow, \downarrow$ ):  $\hat{a}_{j\tau}^\dagger |0\rangle = |u_j\rangle |\tau\rangle$  at different sublattices  $j = 1, 2, 3$ . In what follows we neglect the dispersion of  $\varepsilon_0(\mathbf{k})$  and set its value to zero. Coefficient  $\gamma_{jl}(\mathbf{k}) = -\sum_{\delta} t_{\delta} e^{i\mathbf{k}\delta}$  is the hopping term between neighboring sites (connected with  $\delta$ ) that belong to different sublattices  $j$  and  $l$  (see Fig.4). Constant  $J_{sd}$  describes the exchange coupling between localized and free electrons (so-called *sd*-exchange), it can be either positive or negative, and without loss of generality we take  $J_{sd} > 0$ .  $\hat{\sigma}$  is the spin operator.

The local band structure obtained by diagonalization of Hamiltonian (6) consists of six bands which, neglecting the *sd*-exchange, are pair-wise (spin-up and spin-down) degenerate. The exchange interaction gives rise to an additional splitting and mixing of bands. As sublattice sites 1, 2 and 3 are equivalent,  $\gamma_{12}(\mathbf{k}) = \gamma_{23}(\mathbf{k}) = \gamma_{31}(\mathbf{k}) = \gamma(\mathbf{k}) < 0$ . In this case the band structure splits into four bands ( $\varepsilon_1 < \varepsilon_2 < \varepsilon_3 < \varepsilon_4$ ):

$$\begin{aligned} \varepsilon_1(\mathbf{k}) &= 2\gamma - J_{sd}S, & \varepsilon_2(\mathbf{k}) &= -\gamma - \sqrt{J_{sd}^2 S^2 + 9\gamma^2}, \\ \varepsilon_3(\mathbf{k}) &= 2\gamma + J_{sd}S, & \varepsilon_4(\mathbf{k}) &= -\gamma + \sqrt{J_{sd}^2 S^2 + 9\gamma^2}. \end{aligned} \quad (7)$$

The states in the bands  $\varepsilon_1, \varepsilon_3$  are nondegenerate, and those in bands  $\varepsilon_2, \varepsilon_4$  are double-degenerate. Corresponding eigen vectors (local spin quantization axis is parallel to  $\mathbf{L}_1$ ) for

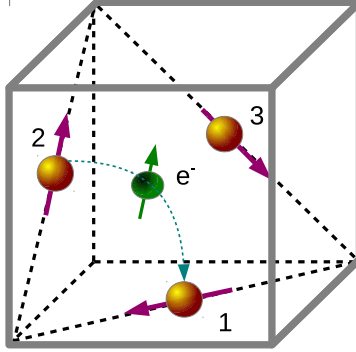


Figure 4. (Color online) Electron ( $e^-$ ) hopping between the magnetic sites. Different sites generate different quantization axes, due to  $120^\circ$  misalignment of local moments. Thus, the hopping electron is always in a superposition of spin-up and spin-down states.

the lower bands  $\varepsilon_1, \varepsilon_2$  are the following:

$$\begin{aligned}
 |\Psi_1\rangle &= \frac{1}{\sqrt{3}} |\uparrow\rangle \left[ |u_1\rangle + \frac{1}{2} (|u_2\rangle - |u_3\rangle) \right] + \frac{1}{2} |\downarrow\rangle (|u_2\rangle + |u_3\rangle), \\
 |\Psi_{2a}\rangle &= |\eta_1\rangle |\uparrow\rangle + |\eta_2\rangle |\downarrow\rangle, \quad |\Psi_{2b}\rangle = |\eta_2\rangle |\uparrow\rangle + |\eta_3\rangle |\downarrow\rangle,
 \end{aligned} \tag{8}$$

where we have introduced the following (non-normalized) combinations of the mutually orthogonal Bloch functions (see Appendix A for details):

$$\begin{aligned}
 |\eta_1\rangle &= \sqrt{\frac{2}{3}} \cos \psi |u_1\rangle - \frac{1}{2\sqrt{6}} (\cos \psi + 3 \sin \psi) (|u_2\rangle - |u_3\rangle), \\
 |\eta_2\rangle &= \frac{1}{2} \sin \left( \psi - \frac{\pi}{4} \right) (|u_2\rangle + |u_3\rangle), \\
 |\eta_3\rangle &= \sqrt{\frac{2}{3}} \sin \psi |u_1\rangle - \frac{1}{2\sqrt{6}} (\sin \psi + 3 \cos \psi) (|u_2\rangle - |u_3\rangle) \\
 \langle \eta_1 | \eta_1 \rangle &= \langle \eta_3 | \eta_3 \rangle = \frac{1}{4} (3 + \sin 2\psi), \quad \langle \eta_2 | \eta_2 \rangle = \frac{1}{4} (1 - \sin 2\psi).
 \end{aligned} \tag{9}$$



The effective parameter  $\psi$  depends on the relation between the  $sd$ -exchange and the hopping integral as follows:

$$\sin 2\psi = \frac{3\gamma}{\sqrt{J_{sd}^2 S^2 + 9\gamma^2}}. \quad (10)$$

It is determined by the band structure and, like in the case of collinear AFM,<sup>17</sup> plays a crucial role in the adiabatic electron dynamics. It describes an overlap of the functions (9),

$$\langle \eta_1 | \eta_3 \rangle = \frac{1}{4} (1 + 3 \sin 2\psi), \quad (11)$$

and hence, the spin tunneling between different sites.

Expressions for the eigen functions  $|\Psi_3\rangle, |\Psi_{4a,b}\rangle$  corresponding to the upper bands  $\varepsilon_3, \varepsilon_4$ , are analogous to those for  $|\Psi_1\rangle, |\Psi_{2a,b}\rangle$  with substitution  $\psi \rightarrow -\psi, \uparrow \leftrightarrow \downarrow$ .

Rather complicated (compared to the case of collinear AFM) structure of the eigenfunctions  $|\Psi_j\rangle$  is due to noncollinearity of neighboring localized moments. As a result, a free electron polarized along, say,  $\mathbf{S}_1$  direction is, after hopping, always in a superposition of spin states with respect to the new host's quantization axis (see Fig.4). It is instructive to analyze the energy spectrum with account of average spin  $\mathbf{s} \equiv \langle \hat{\boldsymbol{\sigma}} \rangle$  of the corresponding eigen state (hereafter we use the convention  $\hbar = 1$ ). As it was already mentioned, in the AFM ground state the magnetization of localized spins  $\mathbf{M} = 0$  and one can anticipate that the ground state of conduction electrons is a spin-less. It can be easily checked from (8) that the lowest energy band ( $\varepsilon_1$ ) corresponds to the zero-spin ‘‘singlet’’ state  $|\Psi_1\rangle$ . Next band in energy scale,  $\varepsilon_2$ , is formed by degenerate states  $|\Psi_{2a}\rangle$  and  $|\Psi_{2b}\rangle$  which are spin-polarized in  $z$  direction parallel to AFM vector  $\mathbf{L}_1$  with opposite spin values  $S_z = \pm(1 + \sin 2\psi)/2$ . In equilibrium ( $\mathbf{M} = 0$ ) both states should be equally populated. The other states that form the upper bands  $\varepsilon_3$  and  $\varepsilon_4$  have analogous properties:  $|\Psi_3\rangle$  is spin-less, and  $|\Psi_{4a}\rangle, |\Psi_{4b}\rangle$  are spin-polarized.

Obviously, in the case of spin-injection only the degenerate states  $|\Psi_{2a}\rangle, |\Psi_{2b}\rangle$  and  $|\Psi_{4a}\rangle, |\Psi_{4b}\rangle$  could be populated and thus can participate in spin transport. Moreover, in the system under consideration the Berry connection of nondegenerate states is proportional to the average spin (see Appendix B) and thus vanishes for  $|\Psi_1\rangle$  and  $|\Psi_3\rangle$ . If, in addition,  $s-d$  exchange coupling is rather strong ( $J_{sd} \gg \gamma$ ), the lower bands  $\varepsilon_1, \varepsilon_2$  are well separated from the upper ones  $\varepsilon_3, \varepsilon_4$ , and the transport of spin-polarized electrons is restricted mainly to the second  $\varepsilon_2$  band.

In what follows we assume that the Fermi level is situated in the vicinity of the degenerate band  $\varepsilon_2$  and in the next section we consider the adiabatic spin dynamics related with tunneling between states  $|\Psi_{2a}\rangle$  and  $|\Psi_{2b}\rangle$  in the AFM texture.

### C. Pseudospin and dynamic equations

We follow the semiclassical approach<sup>17,33-35</sup> to describe the effective electron dynamics in the degenerate band  $\varepsilon_2$ . An individual electron is seen as a wave-packet

$$|W\rangle = \int d\mathbf{k} p(\mathbf{k} - \mathbf{k}_c) [c_a |\Psi_{2a}\rangle + c_b |\Psi_{2b}\rangle], \quad (12)$$

where  $\int d\mathbf{k} |p(\mathbf{k} - \mathbf{k}_c)|^2 = \mathbf{k}_c$  is the center of mass momentum,  $\langle W | \mathbf{r} | W \rangle = \mathbf{r}_c$  is the center of mass position,  $|c_a|^2 + |c_b|^2 = 1$ . We assume that the wave-packet (12) spreads small compared to the length-scale of AFM inhomogeneity.

Coherent dynamics between the two subbands introduces an internal degree of freedom which we describe by the spinor  $(c_a c_b)$  or, equivalently, by the isospin vector

$$\mathbf{C} = \{2\text{Re}(c_a c_b^*), -2\text{Im}(c_a c_b^*), |c_a|^2 - |c_b|^2\}, \quad (13)$$

It is worth to mention that both the spinor and the normalized isospin vector  $\mathbf{C}$  represent  $SU(2)$  group in 2-dimensional Hilbert space formed by the state vectors  $|\Psi_{2a}\rangle$  and  $|\Psi_{2b}\rangle$ .

Space-time dependence of the state vectors  $|\Psi_{2a}\rangle$  and  $|\Psi_{2b}\rangle$  stems exclusively from the rotation of the local spin quantization axis induced by variation of the AFM moments  $(\mathbf{S}_j(t, \mathbf{r}_c))$  or, equivalently,  $\mathbf{L}_1(t, \mathbf{r}_c), \mathbf{L}_2(t, \mathbf{r}_c), \mathbf{n}(t, \mathbf{r}_c)$ . It should be noted that the space dependence of Bloch functions  $|u_j\rangle$  is substantial only at the lengthscale of interatomic distances and thus is unimportant at the large-scale variations of the AFM order parameters. Since, in addition, we neglect spin-orbit interactions, rotation of the magnetic moments is decoupled from variation of the crystallographic axes and, correspondingly, spin and space-dependent states of the carriers are disentangled.

As the local orientation of the AFM moments is unambiguously defined by the rotation matrix  $\mathfrak{R}(\boldsymbol{\varphi})$  (see (3)), the state vector  $|\Psi_{2a,b}(r_\mu)\rangle$  at a given point  $r_\mu = (t, \mathbf{r}_c)$  can be defined by a  $SU(2)$  gauge unitary transformation corresponding to  $O(3)$  rotation:

$$\hat{U} = \cos \frac{\theta}{2} \hat{1} - i \sin \frac{\theta}{2} \mathbf{N} \hat{\boldsymbol{\sigma}} = \frac{1}{\sqrt{1 + \boldsymbol{\varphi}^2}} (\hat{1} - i \boldsymbol{\varphi} \hat{\boldsymbol{\sigma}}). \quad (14)$$

Thus,

$$|\Psi_2(r_\mu)\rangle = \hat{U} |\Psi_2(r_\mu^0)\rangle \quad (15)$$

where the reference state vectors  $|\Psi_2(r_\mu^0)\rangle$  and reference AFM vectors  $\mathbf{L}_1^{(0)}, \mathbf{L}_2^{(0)}$  are taken in the same fixed point  $r_\mu^0$ . The gauge is fixed by the choice of spin eigenstates at this point<sup>36</sup>.

The vectors  $|\Psi_{2a}\rangle$  and  $|\Psi_{2b}\rangle$  also depend indirectly on quasi-wave-vector  $k_\mu = (0, \mathbf{k}_c)$  through the coefficient  $\psi[\gamma(\mathbf{k}_c)]$ .

According to the general theory,<sup>34</sup> the set of equations of motion for the dynamic variables  $\mathbf{r}_c$ ,  $\mathbf{k}_c$  and  $\mathbf{C}$  can be written as follows (see Ref. 17 for the detailed derivation):

$$\dot{\mathbf{C}} = 2\mathbf{C} \times \left( \mathbf{A}_\mu^r \dot{r}_\mu + \mathbf{A}_\mu^k \dot{k}_\mu \right), \quad (16)$$

$$\dot{k}_\mu = -\partial_\mu^r \varepsilon_2 + \mathbf{C} \left( \mathbf{R}_{\mu\nu}^{rr} \dot{r}_\nu + \mathbf{R}_{\mu\nu}^{rk} \dot{k}_\nu \right), \quad (17)$$

$$\dot{r}_\mu = \partial_\mu^k \varepsilon_2 - \mathbf{C} \left( \mathbf{R}_{\mu\nu}^{kr} \dot{r}_\nu + \mathbf{R}_{\mu\nu}^{kk} \dot{k}_\nu \right), \quad (18)$$

where the gauge potentials  $\{\mathbf{A}_\mu^r, \mathbf{A}_\mu^k\}$ , Berry connection  $\hat{\mathcal{A}}_\mu^\alpha \equiv \mathbf{A}_\mu^\alpha \hat{\boldsymbol{\sigma}}$ , and Berry curvatures  $\mathbf{R}_{\mu\nu}^{\alpha\beta}$  ( $\alpha, \beta = r, k$ ) are introduced in a standard way as

$$\hat{\mathcal{A}}_\mu^\alpha = i \begin{pmatrix} \langle \Psi_{2a} | \partial_\mu^\alpha \Psi_{2a} \rangle & \langle \Psi_{2a} | \partial_\mu^\alpha \Psi_{2b} \rangle \\ \langle \Psi_{2b} | \partial_\mu^\alpha \Psi_{2a} \rangle & \langle \Psi_{2b} | \partial_\mu^\alpha \Psi_{2b} \rangle \end{pmatrix}, \quad (19)$$

$$\mathbf{R}_{\mu\nu}^{\alpha\beta} = \partial_\mu^\alpha \mathbf{A}_\nu^\beta - \partial_\nu^\beta \mathbf{A}_\mu^\alpha + 2\mathbf{A}_\mu^\alpha \times \mathbf{A}_\nu^\beta. \quad (20)$$

Starting from equation (16) we drop the subscript  $c$  on  $\mathbf{r}_c$  and  $\mathbf{k}_c$ .

### III. ADIABATIC DYNAMICS

#### A. Berry curvature and topology of AFM texture

Before considering the possible dynamics of free electrons it is instructive to analyze the explicit expressions for the Berry connection and the Berry curvature in AFM texture. Calculations based on definitions (19), (20) (see Appendix B) show that the gauge potential

$$\mathbf{A}_\mu^r = \frac{1}{4} \mathfrak{R}^{-1}(\varphi) [(1 + \sin 2\psi) \boldsymbol{\Omega}_\mu - (1 - \sin 2\psi) \mathbf{n} (\boldsymbol{\Omega}_\mu \mathbf{n})], \quad (21)$$

and  $\mathbf{A}_\mu^k = 0$  in the absence of spin-orbit interactions.<sup>17</sup> Correspondingly, nontrivial components of the Berry curvature are the following

$$\begin{aligned} \mathbf{R}_{\mu\nu}^{rr} &= \frac{1}{8} (1 - \sin 2\psi) \mathfrak{R}^{-1}(\varphi) [2(1 + \sin 2\psi) \boldsymbol{\Omega}_\nu \times \boldsymbol{\Omega}_\mu - (3 + \sin 2\psi) \mathbf{n} (\mathbf{n} \cdot \boldsymbol{\Omega}_\nu \times \boldsymbol{\Omega}_\mu)], \\ \mathbf{R}_{\mu\nu}^{rk} &= -\mathbf{R}_{\nu\mu}^{kr} = \frac{1}{4} \partial_\nu^k \sin 2\psi \mathfrak{R}^{-1}(\varphi) [\boldsymbol{\Omega}_\mu + \mathbf{n} (\boldsymbol{\Omega}_\mu \mathbf{n})]. \end{aligned} \quad (22)$$

The multiplier  $\mathfrak{R}^{-1}(\boldsymbol{\varphi})$  (inverse rotation matrix) in (21), (22) results from the gauge covariance of the non-Abelian gauge fields. As we will see later, the same rotation relates the isospin to the real spin.

Analysis of the relations (21), (22) shows that the gauge potentials produced by the AFM texture depend on the orientation of AFM vectors through the rotation vector  $\boldsymbol{\Omega}_\mu$  which, in turn, is related to the dynamic magnetization  $\mathbf{M}_{\text{dyn}}$ . The Berry curvature  $\mathbf{R}_{\mu\nu}^{rr}$  for *free electron* is proportional to the curvature  $\mathbf{K}_{\mu\nu} \equiv \boldsymbol{\Omega}_\mu \times \boldsymbol{\Omega}_\nu = \partial_\mu^r \boldsymbol{\Omega}_\nu - \partial_\nu^r \boldsymbol{\Omega}_\mu$  of the *AFM texture*<sup>43</sup>. In other words, the Berry curvature is intimately related with topological properties of the space distribution of the localized moments. To give an example distribution with the nontrivial curvature, we note that in elasticity theory  $K_{\mu\nu} \neq 0$  is called bend-twist tensor. So, one can imagine that in some toroidal area (see Figs.5,8) the orientation of AFM vectors is obtained by two rotations – one, around the in-plane axis tangent to the torus (twist with the rotation vector  $\boldsymbol{\varphi}_1$ ), and another, around the vertical torus axis  $z$  (bend with the rotation vector  $\boldsymbol{\varphi}_2$ ). The curvature vector  $\mathbf{K}_{xy} = \boldsymbol{\Omega}_x \times \boldsymbol{\Omega}_y$  in each point of the structure is directed along the radius. This structure, through *sd*-exchange, forms a potential with a Berry curvature  $\mathbf{R}_{xy}^{rr} \propto \mathbf{K}_{xy}$  and produces a “Lorentz-like” effective force for free spin-polarized electrons, as will be explained below.

It is instructive to compare Expr. (21) describing a gauge potential in AFM with the analogous expression<sup>37</sup> for a ferromagnetic material with the magnetization vector  $\mathbf{m}$ :

$$\mathbf{A}_\mu^{FM} = -\mathbf{m} \times \partial_\mu^r \mathbf{m} = -(1 - \mathbf{m} \otimes \mathbf{m}) \boldsymbol{\Omega}_\mu. \quad (23)$$

Although in ferromagnets the gauge transformation is applied to the real spin (not to isospin), and the gauge potential is Abelian, comparison of expressions (23) and (21) shows that up to the details related with peculiarities of electron hopping, geometric effects in FM and AFM are related with the “dynamic” magnetization proportional to the angular velocity  $\boldsymbol{\Omega}_\mu$ .

It is also worth to note the relation between the curvature  $\mathbf{K}_{\mu\nu}$  and the topological properties of localized nonlinear magnetic structures: skyrmions, solitons, vortecies. For example, the topological charge of a two-dimensional (in the real space) skyrmion, that counts how many times the vector order parameter  $\mathbf{m}(t, \mathbf{r})$  wraps around the unit sphere, is defined as:<sup>38</sup>

$$Q = \frac{1}{8\pi} \int \mathbf{m} \cdot (\partial_\mu \mathbf{m} \times \partial_\nu \mathbf{m} - \partial_\nu \mathbf{m} \times \partial_\mu \mathbf{m}) dx_\mu dx_\nu. \quad (24)$$

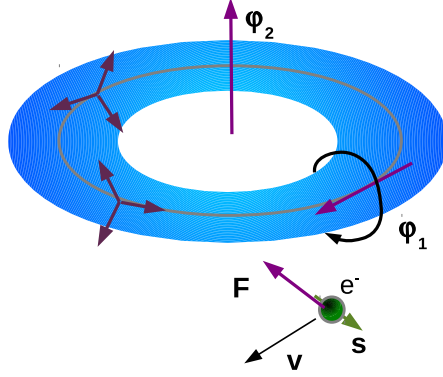


Figure 5. (Color online) Orbital dynamics of an electron in the AFM texture with nonzero curvature. Blue (shadowed) torus shows the area with twisted (vector  $\varphi_1$ ) and bended (vector  $\varphi_2$ ) AFM vectors (three bounded arrows). Free spin-polarized (spin  $\mathbf{s}$ ) electron moving in this area with the group velocity  $\mathbf{v}$  feels the effective force  $\mathbf{F}$ , see text for details.

With the use of the relations (3), (4), and (5) it can be easily shown that  $Q$  is proportional to the projection of the curvature vector  $\mathbf{K}_{\mu\nu}$  onto the order parameter  $\mathbf{m}$  averaged over space:

$$Q = \frac{1}{4\pi} \int (\mathbf{m} \cdot \boldsymbol{\Omega}_\mu \times \boldsymbol{\Omega}_\nu) dx_\mu dx_\nu. \quad (25)$$

The relation (25) is applicable to any magnetic system with the vector order parameter: a ferromagnet, with  $\mathbf{m}$  playing the role of magnetization vector, a collinear AFM, where  $\mathbf{m}$  corresponds to the Néel vector.

Topological charges of the three-dimensional structures with the vector order parameter are characterized with the Hopf's invariant<sup>39,40</sup> which describes  $S^3$  to  $S^2$  map:

$$H = \frac{1}{16\pi^2} \int dx^3 \varepsilon_{\mu\nu\gamma} \varepsilon_{jklm} \nu_j \frac{\partial \nu_k}{\partial x_\mu} \frac{\partial \nu_l}{\partial x_\nu} \frac{\partial \nu_m}{\partial x_\gamma}, \quad (26)$$

where the four-component vector  $(\boldsymbol{\nu}, \nu_4)$  is related with the Gibb's vector  $\boldsymbol{\varphi} = \boldsymbol{\nu}/\nu_4$ ,  $\nu_4 =$

$\cos \theta/2$ ,  $\varepsilon_{\mu\nu\gamma}$  and  $\varepsilon_{jklm}$  are fully antisymmetric tensors.

For the case of noncollinear AFMs an appropriate topological invariant is given by the expressions<sup>41</sup>

$$Q = -\frac{1}{24\pi^2} \int dx^3 \varepsilon_{\mu\nu\gamma} \text{Tr} \left[ \mathfrak{R}^{-1}(\boldsymbol{\varphi}) \frac{\partial}{\partial x_\mu} \mathfrak{R}(\boldsymbol{\varphi}) \mathfrak{R}^{-1} \frac{\partial}{\partial x_\nu} \mathfrak{R}(\boldsymbol{\varphi}) \mathfrak{R}^{-1} \frac{\partial}{\partial x_\gamma} \mathfrak{R}(\boldsymbol{\varphi}) \right], \quad (27)$$

which corresponds to  $S^3$  to  $S^3$  map. Three-dimensional AFM order parameter (formed by mutually orthogonal  $\mathbf{L}_1$  and  $\mathbf{L}_2$  vectors) is parametrized with the rotational tensor  $\mathfrak{R}(\boldsymbol{\varphi})$ . With the use of expressions (4) the topological invariant (27) can be expressed in terms of the rotation vectors  $\boldsymbol{\Omega}_\mu$  as follows:

$$Q = -\frac{1}{24\pi^2} \int dx^3 \varepsilon_{\mu\nu\gamma} (\boldsymbol{\Omega}_\mu \cdot \boldsymbol{\Omega}_\nu \times \boldsymbol{\Omega}_\gamma). \quad (28)$$

It can be easily seen that, in analogy with ferromagnets, the topological charge (28) is proportional to the projection of the curvature vector  $\mathbf{K}_{\nu\gamma}$  onto direction of dynamics magnetization  $\boldsymbol{\Omega}_\mu$  seen by the free electron moving in  $x_\mu$  direction.

Note that the model “twist-bend” structure shown in Figs.5,8 can, in principle, have nonzero topological charge if the the AFM ordering outside the toroidal area is homogeneous. In this case the structure is characterized with three nontrivial noncollinear rotational vectors:  $\boldsymbol{\Omega}_1$  and  $\boldsymbol{\Omega}_2$  for twisting and bending and  $\boldsymbol{\Omega}_3$  that describes smooth rotation of AFM vectors in the intermediate area between torus and infinity.

## B. Free spin dynamics and gauge potential

Let us consider a typical spintronic problem in which a nonequilibrium spin-polarized carrier is injected into an AFM. The question is: “Does the AFM medium affects the state of an electron? If it does, how could this effect be observed?”

To begin with, we find the relation between the isospin vector  $\mathbf{C}$  (which itself is not gauge invariant and depends upon the choice of the eigen functions  $|\Psi_{2a}\rangle$ ,  $|\Psi_{2b}\rangle$ ) and the observable (and fully gauge invariant) spin  $\mathbf{s} \equiv \langle W | \hat{\boldsymbol{\sigma}} | W \rangle$ . Direct calculations based on the states (8), (15) give rise to the following expression for spin vector:

$$\mathbf{s}(t, \mathbf{r}) = \frac{1}{2} (1 + \sin 2\psi) [\mathfrak{R}(\boldsymbol{\varphi}) \mathbf{C}] - \frac{1}{2} (1 - \sin 2\psi) (\mathfrak{R}(\boldsymbol{\varphi}) \mathbf{C} \cdot \mathbf{n}) \mathbf{n}. \quad (29)$$

Using normalization of the isospin,  $|\mathbf{C}|^2 = 1$ , we arrive at a relation between the spin of free carrier and the orientation of the plane formed by the localized spins and represented by the

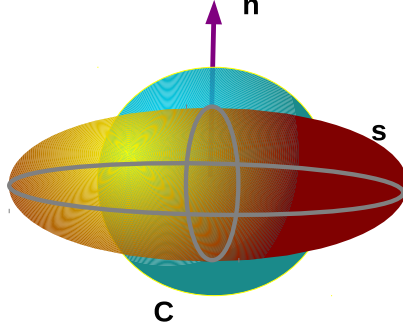


Figure 6. (Color online) Isospin  $\mathbf{C}$  (sphere) and real spin  $\mathbf{s}$  (spheroid) in the local frame.

vector  $\mathbf{n}(t, \mathbf{r})$  (see Fig.6):

$$\frac{(\mathbf{ns})^2}{\sin^2 2\psi} + \frac{4(\mathbf{n} \times \mathbf{s})^2}{(1 + \sin 2\psi)^2} = 1. \quad (30)$$

Analysis of expression (30) shows that, like in the case of a collinear AFM<sup>17</sup> (see also Eq.(38)), spin polarization of the conduction electron depends upon the orientation of the AFM vectors. In a noncollinear AFM the vector  $\mathbf{s}$  varies on an oblate spheroid (on a prolate in the collinear AFM), the short axis of which coincides with the plane normal. Like in the collinear case,  $\mathbf{s}^2 \leq 1$ , which means that an electron is in a mixed spin state due to entanglement between the space and spin degrees of freedom.

Equation for spin dynamics obtained from (29) with account of (16) and (21) (see Appendix B for hints of the derivation) is similar to the Euler's equation for rotation of a rigid body:

$$\dot{\mathbf{s}} - \boldsymbol{\Omega} \times \mathbf{s} = -\sin 2\psi \boldsymbol{\Omega} \times \hat{g}\mathbf{s}, \quad (31)$$

where we introduced the tensor

$$\hat{g} = \hat{1} + \left[ \left( \frac{1 + \sin 2\psi}{2 \sin 2\psi} \right)^2 - 1 \right] \mathbf{n} \otimes \mathbf{n}, \quad (32)$$

and, as it was already noted,  $\boldsymbol{\Omega} = \boldsymbol{\Omega}_t + \boldsymbol{\Omega}_l \dot{r}_l$ . The second term on the l.h.s. of Eq. (31) originates from the rotation of the local frame associated with vectors  $\mathbf{L}_1, \mathbf{L}_2, \mathbf{n}$  (for the constant isospin  $\mathbf{C}$ ). In analogy with Ref.33, it could be called “tracking” term because it reflects the tendency of the AFM lattice to drag the electron spin along with the time/space AFM motion.

The r.h.s. describes the spin evolution in the local frame due to accumulation of a  $SU(2)$  non-Abelian Berry phase. Namely, spin vector rotates around the angular velocity  $\boldsymbol{\Omega}$  being simultaneously bounded to the spheroid (30). Thus, Eq. (31) is the Bloch equation for spin precession in the effective magnetic field  $\mathbf{H}^{eff} = -\sin 2\psi \hat{g} \boldsymbol{\Omega}$ . As  $\boldsymbol{\Omega}$  is proportional to the dynamic magnetization  $\mathbf{M}_{\text{dyn}}$  of the AFM layer, the origin of the effective magnetic field  $\mathbf{H}^{eff}$  acting on free spins has the same nature as in ferromagnets.<sup>42</sup>

It should be stressed that spin dynamics substantially depends upon the strength of  $sd$ -exchange coupling. In the limit  $J_{sd} \rightarrow 0$  (which means that  $\sin 2\psi \rightarrow 1$ ), the electron spin coincides with the pseudospin  $\mathbf{C}$  up to rotation  $\mathfrak{R}(\boldsymbol{\varphi})$  and  $\dot{\mathbf{s}} = 0$ . In the opposite case of extremely strong  $J_{sd} \rightarrow \infty$  (or, equivalently,  $\sin 2\psi \rightarrow 0$ ) the r.h.s. term in equation (31) vanishes. So, in the case of strong coupling between free and localized spins the free spin simply tracks orientation of the local frame in each point.

Orbital dynamics of the wave-packet (12) is described by semiclassical equations obtained from (17), (18) with account of (31) as follows:

$$\dot{r}_\mu = \partial_\mu^k \varepsilon_2 + \frac{1}{2} \partial_\mu^k \ln(1 + \sin 2\psi) \left[ \mathbf{s} \cdot \boldsymbol{\Omega} + \frac{1}{\sin 2\psi} (\mathbf{n} \cdot \mathbf{s})(\mathbf{n} \cdot \boldsymbol{\Omega}) \right], \quad (33)$$

$$\dot{k}_\mu = -\partial_\mu^r \varepsilon_2 - \frac{1}{2} \dot{\mathbf{s}} \cdot \boldsymbol{\Omega}_\mu. \quad (34)$$

The spin-dependent addition to the group velocity in Eq. (33) is proportional to  $\partial_\mu^k \varepsilon_2$ , because  $\partial_\mu^k \sin 2\psi \sim \partial_\mu^k \gamma \sim \partial_\mu^k \varepsilon_2$ . So, coupling between the free and the localized spins in the rotated AFM texture results in “renormalization” of the effective electron mass. An analogous term, omitted in (34) for the sake of simplicity, appears also in the equation for acceleration (see Appendix B, Eq.(B7)).

The nontrivial, spin-dependent term on the r.h.s of Eq. (34) is intimately related to the spin dynamics. It can also be represented in the form of a fictitious Lorentz force with the



effective electric-like,  $E_\mu$ , and magnetic-like,  $B_\xi$  components:

$$\dot{k}_\mu = -\partial_\mu^r \varepsilon_2 + q (E_\mu + \varepsilon_{\mu\nu\xi} \dot{r}_\nu B_\xi), \quad (35)$$

$$qE_\mu = \frac{1}{2} [\mathbf{s} \cdot \boldsymbol{\Omega}_t \times \boldsymbol{\Omega}_\mu + \sin 2\psi \hat{g} \mathbf{s} \cdot \boldsymbol{\Omega}_t \times \boldsymbol{\Omega}_\mu], \quad (36)$$

$$qB_\xi = \frac{1}{2} \varepsilon_{\xi\mu\nu} [\mathbf{s} \cdot \boldsymbol{\Omega}_\nu \times \boldsymbol{\Omega}_\mu + \sin 2\psi \hat{g} \mathbf{s} \cdot \boldsymbol{\Omega}_\nu \times \boldsymbol{\Omega}_\mu], \quad (37)$$

where, as above,  $\varepsilon_{\xi\mu\nu}$  is the antisymmetric Levi-Civita tensor. The corresponding effective “charge”  $q$  (field “source”) is proportional to the spin<sup>45</sup>.

Equations (35), (36), and (37) are similar to equations that describe an orbital motion of individual electron in a collinear AFM.<sup>17</sup> In both cases the gauge charge  $q$  depends upon the spin which, according to equation (31), shows its own dynamics and thus can vary in time. In both cases the gauge charge depends upon the  $sd$ -exchange constant (in our case, through the multiplier  $\sin 2\psi$ ) and vanishes when  $J_{sd} \rightarrow 0$ .

The new feature demonstrated in this paper is certain universality of spin-dependent orbital dynamics in AFMs. Really, the dynamic equations of a collinear AFM ( Eqs.(8) of Ref.17) have practically the same form as equations (31), (33), and (34) of the present paper when written in terms of angular velocity  $\dot{\mathbf{L}} = \boldsymbol{\Omega} \times \mathbf{L}$ :

$$\dot{\mathbf{s}} - \boldsymbol{\Omega} \times \mathbf{s} = -\boldsymbol{\Omega} \times \hat{g} \mathbf{s}, \quad \hat{g} = \hat{1} + (\xi^2 - 1) \mathbf{L} \otimes \mathbf{L}, \quad (38)$$

$$\dot{r}_\mu = -\partial_\mu^k \varepsilon_2 + \frac{1}{2} \partial_\mu^k \ln \xi [\mathbf{s} \cdot \boldsymbol{\Omega} - (\mathbf{L} \cdot \mathbf{s}) (\mathbf{L} \cdot \boldsymbol{\Omega})], \quad (39)$$

$$\dot{k}_\mu = -\frac{1}{2} \boldsymbol{\Omega}_\mu \cdot \dot{\mathbf{s}}, \quad (40)$$

where  $\xi$ , in the original notations, is the overlap of the wave functions analogous to  $\sin 2\psi$  of the present paper (see Eq.(10)), and notations  $\mathbf{L}$  is used for the Néel vector of collinear AFM.

Thus, in AFMs with strong exchange coupling between the magnetic sublattices the emergent Lorentz force (35) is defined by the *angular velocity*  $\boldsymbol{\Omega}_t$  (and hence, the dynamic magnetization) and the *AFM curvature*  $\boldsymbol{\Omega}_\nu \times \boldsymbol{\Omega}_\mu$ , no matter how complicated or simple the magnetic structure is. The details of the structure (number of sublattices, dimensionality, type, mutual orientation) reveal themselves in a cumbersome presentation of the gauge charge, tensor  $\hat{g}$  and spin ellipsoid: in a collinear AFM the anisotropy of these parameters is dictated by the easy-axis parallel to a single AFM vector, in the present case – by the easy-plane formed by two orthogonal Néel vectors.

The effective electric field (36) plays a role of a spin-dependent motive force (similar to that in FM, see Ref. 18). So, an oscillating ( $\Omega_t \neq 0$ ) inhomogeneous ( $\Omega_\mu \neq 0$ ) AFM structure can produce an electric current (or voltage) and thus can be observed by standard electric measurements.

The effective magnetic field (37) is proportional to the projection of curvature  $\Omega_\nu \times \Omega_\mu$  of the AFM texture on the free spin  $\mathbf{s}$ . Direction of the latter correlates (and in the limit of strong *sd*-exchange coupling, coincides) with the direction of  $\Omega$  and dynamic magnetization of the AFM. Thus, the flux of the emergent magnetic field is related with the topological charge of the AFMs distribution (see Eq. (28) where the curvature is projected on the direction of dynamic magnetization seen by the free electron). An analogous situation takes place in skyrmions where the flux of emergent magnetic field is associated with skyrmion number (i.e., topological charge).<sup>38</sup> However, gauge effects in skyrmions and AFMs are principally different. Namely, a skyrmion can be treated as a ferromagnet with a complicated distribution of localized moments, and in adiabatic limit the spin of a conduction electron always tracks the local orientation of magnetization; gauge potential is Abelian; topological charge of skyrmion is related with chirality.<sup>15</sup> In contrast, the AFM which we consider here has zero total static magnetization; complicated slowly varying magnetic texture is locally formed by a proper number of AFM vectors attributed to same point; a conduction electron feels the local frame induced by magnetic moments but not the direction of magnetization itself. Nontrivial effect of geometric phase in absence of total magnetization is due to the *degeneracy of states* and resulting *non-Abelian* character of the gauge potential.

The emergent magnetic field in adiabatic motion is usually associated with topological Hall effect. On the other hand, most AFM structures are usually invariant with respect to time reversal symmetry and this forces Hall conductivities to vanish. Recently, it was demonstrated that noncollinear<sup>10</sup> and frustrated<sup>44</sup> AFMs can show anomalous Hall effect that arises due to spin-orbit coupling. The origin of nonzero Hall conductivity in these materials is the *Berry curvature* in *momentum* space. In contrast, equation (35) (and the analogous equation for collinear AFM from Ref. '17) shows that Hall effect can in principle be observed in compensated AFMs with negligible spin-orbit coupling. In this case the Hall conductivity originates from the *Berry curvature* in *real* space and, what is also important, is related with the *curvature of the AFM texture*. The required breaking of time-reversal symmetry results from the inhomogeneity<sup>47</sup> and related dynamic magnetization  $\mathbf{M}_{\text{dyn}} \sim \Omega$

of AFM structure as was explained above. Following Ref. 12 this Hall effect should be called topological.

Equations (31), (33), and (34) state the main result of this paper. They describe electron dynamics in a noncollinear AFM in terms of three observables ( $\mathbf{s}, \mathbf{r}, \mathbf{k}$ ). However, so far our treatment was quite general and abstract. To make physical meaning of the obtained results clearer, in the next Section I consider some special cases accessible for the experimental implementation.

## IV. EXAMPLES

### A. Travelling between AFM domains

Let us start from the “canonical” example of an AFM texture – flat, one-dimensional domain wall separating two domains with different orientation of spin-ordering plane (see Fig.7).

For the definiteness I consider domains related by a rotation around the cubic axis through  $90^\circ$  (corresponding rotation matrix is  $\mathfrak{R}_{12}$ ). Let us suppose that AFM film is connected to two ferromagnetic electrodes that can produce a spin-polarized current (with the spin vector  $\mathbf{s}_0$ ) in the in-plane geometry. The thickness of the AFM layer is smaller or comparable with the spin-coherence length (to exclude spin scattering processes), the thickness of the domain wall is much larger than the lattice constant (to validate the adiabatic approximation). Electric voltage applied to the system initiates an electron flow between the ferromagnetic electrodes with an average constant velocity  $\mathbf{v}$  directed along the domain wall normal (denoted as  $x$  axis). As the curvature of the flat domain wall is zero, the AFM texture affects only the spin evolution described by Eq. (31) which can be rewritten in the following form:

$$\frac{d\mathbf{s}}{dx} = \boldsymbol{\Omega}_x \times (\mathbf{s} - \sin 2\psi \hat{g}\mathbf{s}), \quad (41)$$

where the rotation vector  $\boldsymbol{\Omega}_x$  has a fixed direction. It follows from Eq.(41) that after travelling through the domain wall vector  $\mathbf{s}$  will change by the value  $\Delta\mathbf{s}$  which consists of two part: rotation with the local AFM frame (due to the first term in parenthesis) and geometric phase rotation (the second term) over spheroid (30). In the case of strong exchange coupling ( $\sin 2\psi \ll 1$ ) the first effect dominates. In this case

$$\Delta\mathbf{s} \approx \mathfrak{R}_{12}\mathbf{s}_0, \quad (42)$$

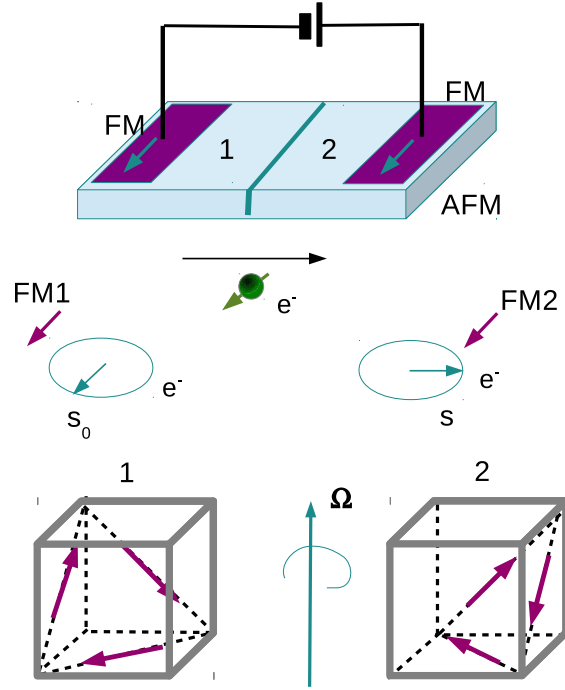


Figure 7. (Color online) Probing the domain wall with the spin-polarized current. Two ferromagnetic electrodes, FM1 and FM2, placed over the AFM film produce spin-polarized current in the in-plane geometry (upper panel). Two AFM domains 1 and 2 (lower panel) are related through the  $90^\circ$  rotation. The spin of the electron  $e^-$  travelling through the domain wall tracks the local AFM structure and rotates (central panel). Misorientation between the free spin and the FM2 magnetization contributes to magnetoresistance and can be detected.

and the spin polarization can evolve by  $90^\circ$ , as shown in Fig.7. If, then, the magnetization  $\mathbf{M}_2$  of the second FM2 electrode is varied by an external magnetic field (as, e.g., in experiments<sup>46</sup>), magnetoresistance between the FM electrodes will also vary depending on  $(\Delta\mathbf{s} \cdot \mathbf{M}_2)$ .

Thus, the AFM domain wall is a “spin-active” (in analogy with optically active) medium. Spin rotation, quantum analogue of the Faraday rotation in optics, results from the competition of two coherent spin states and could be observed by the electrical measurements.

## B. Enveloping a soliton

Equations (31) and (34) predict nontrivial spin-induced orbital dynamics in a curved AFM texture. As an example, let us consider spin-polarized electrons travelling through a region with the inhomogeneous distribution of AFM vectors obtained in the following way. Suppose, we start from the one-dimensional distribution of AFM vectors described by the Gibb's vector  $\varphi_1 = \tan(\theta_1(\xi)/2) \mathbf{e}_y$  (a "wire" with twisted AFM structure, Fig.8a). Next, the "wire" is bended to make a ring, this corresponds to a rotation with Gibb's vector  $\varphi_2 = \tan(\theta_2(x, y)/2) \mathbf{e}_z$ , where  $\theta_2(x, y) = \tan^{-1} y/x$  (Fig.8b). The resulting rotation  $\varphi = \varphi_2 \circ \varphi_1$  is a composition of twisting and bending:

$$\varphi = \varphi_2 \circ \varphi_1 = \tan \frac{\theta_1(\xi)}{2} \mathbf{e}_y + \tan \frac{\theta_2(x, y)}{2} \mathbf{e}_z - \tan \frac{\theta_1(\xi)}{2} \tan \frac{\theta_2(x, y)}{2} \mathbf{e}_x. \quad (43)$$

The effective coordinate of the first rotation,  $\xi = y \cos \theta_2 - x \sin \theta_2$  bends with the "wire". Such a texture has a nonzero curvature parallel to the radial component  $\mathbf{e}_r$  :

$$\mathbf{K}_{xy} \equiv \boldsymbol{\Omega}_x \times \boldsymbol{\Omega}_y = -\partial_\xi \theta_1(\xi) \sin 2\theta_2 \frac{\mathbf{e}_r}{r}, \quad (44)$$

where  $r$  is the radial coordinate<sup>48</sup>.

Let us further assume that the first, unbended distribution  $\theta_1(\xi)$  corresponds to a kink or two "head-to-head" domain walls separating domains A and B. In this case  $\partial_\xi \theta_1(\xi) \neq 0$  in the vicinity of the domain wall localization. For the definiteness we assume that the domain walls are centered at  $\theta_2 = \pi/4$  (domain wall between A and B) and  $\theta_2 = 5\pi/4$  (domain wall between A and B, see Fig.8c). Obviously,  $\partial_\xi \theta_1(\xi) \neq 0$  has opposite signs in these points. As a result, curvature  $\mathbf{K}_{xy} \neq 0$  along the line  $x = y$  and has the same direction at all points.

According to Eq. (37), AFM curvature produces fictious out-of plane magnetic field

$$qB_z = \frac{1}{2r} \partial_\xi \theta_1(\xi) \sin 2\theta_2 [\mathbf{e}_r \cdot \mathbf{s} + \sin 2\psi \mathbf{e}_r \cdot \hat{\mathbf{g}}\mathbf{s}]. \quad (45)$$

So, spin-polarized electrons with  $\mathbf{s} \parallel \mathbf{K}_{xy}$  travelling with constant velocity  $\mathbf{v} \perp \mathbf{K}_{xy}$  through the texture are exerted by the Lorentz force and deflect from the initial trajectory<sup>?</sup> (see Fig.8c).

As the curvature direction is constant, all equally polarized electrons will deflect in the same way thusdemonstrating a topological spin Hall effect. So, such a texture can be probed with spin-polarized current. On the other hand, electrons with different spins are deflected

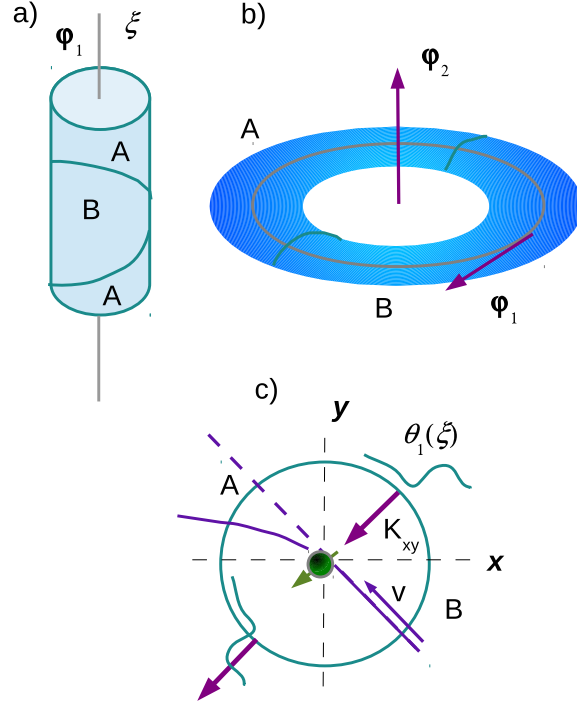


Figure 8. (Color online) Electron traveling in the neighborhood of an AFM soliton. a) “twisting” of an AFM structure (one dimensional rotation with the Gibb’s vector  $\varphi_1$ ); b) “bending” of twisted structure; c) spin-polarized electron moving with velocity  $\mathbf{v}$  feels a Lorentz force at the points of maximal curvature  $\mathbf{K}_{xy}$  (arrows). A and B symbolize different domains.

in opposite directions, so, the texture can also work as a spin-separator. It should be stressed that the topological spin Hall effect can be modified by spin-orbit interaction neglected in the present calculations.

## V. CONCLUSIONS

In the present paper I consider the adiabatic dynamics of free electrons in AFM with triangular magnetic structure. I show that, in analogy with the collinear AFM,<sup>17</sup> the dynamics of a real spin  $\mathbf{s}$  is influenced by space/time variation of antiferromagnetically coupled vectors  $\mathbf{S}_j(\mathbf{r}, t)$ . The main features of the electron behavior arising from accumulation of non-Abelian SU(2) Berry phase: precession of the electron spin around the dynamic AFM magnetization and spin-dependent orbital dynamics, – are similar in both cases. The first

effect is of pure geometric nature, as the homogeneous AFM has no uncompensated magnetization and produces no magnetic field. The second effect is related with processes of spin-pumping and spin-transfer torque and thus experimentally observable.

Similarity (up to the details) of free electron dynamics in the collinear and triangular AFMs gives the grounds to anticipate analogous effects in even more complicated AFM metals like FeMn which shows  $3\mathbf{q}$  structure described in terms of four magnetic sublattices.

The described toy model can be applied to antiperovskites  $\text{Mn}_3\text{MN}$  ( $\text{M}=\text{Ni}, \text{Ag}, \text{Zn}$ ) which show a noncollinear  $120^\circ$  magnetic structure and semiconducting type of conductivity (see, e.g. Ref.49). Although in this paper we appeal mainly to the perovskites  $\text{Mn}_3\text{XN}$ , the results obtained could be applied to the metallic AFM  $\text{IrMn}_3$  with the same triangular structure<sup>50,51</sup> which is widely used in spintronics due to its high Néel temperature.

The influence of the spin-related curvature on the orbital motion of free electron related with topological features of the system and thus is quite a general property. It can be used for detection of inhomogeneous distribution of magnetic systems like topological solitons and/or skyrmions recently observed in AFMs.<sup>52</sup> Adiabatic spin transport is a possible tool for study of AFM 2D and 3D textures induced by mechanical tilting through the flexomagnetic effect typical for triangular AFM structures.<sup>26</sup> A system of triangular Ising spins realized with trapped ions<sup>53</sup> can also be used as a playground for quantum simulation of non-Abelian  $\text{SU}(2)$  Berry-phase effects.

## ACKNOWLEDGMENTS

I am grateful to Yu. Mokrousov, F. Freimut and J. Sinova for fruitful discussions. I also acknowledge help from P. Buhl and A. Malysenko.

## Appendix A: Hamiltonian diagonalization

Hamiltonian (6) mixes all six wavefunctions  $|u_j\rangle|\tau\rangle, j = 1, 2, 3, \tau = \uparrow, \downarrow$ . However, symmetry considerations make it possible to simplify the diagonalization procedure which we describe in this section.

First, we notice that if the quantization axis is taken in the local frame with  $z'_j$  axis parallel to  $\mathbf{S}_j$ , then, the  $sd$ -exchange-term is diagonal in the spin space:  $\mathbf{S}_j \hat{\sigma}_{\tau\tau'} = S \hat{\sigma}_{jz'}$ .

As the vectors  $\mathbf{S}_j$  (and correspondingly local quantization axes) could be generated from the lab axis by rotations around the plane normal  $\mathbf{n}$  it is convenient to introduce new creation/annihilation operators

$$\begin{pmatrix} \hat{b}_{j\uparrow} \\ \hat{b}_{j\downarrow} \end{pmatrix} = \hat{U}_j^\dagger \begin{pmatrix} \hat{a}_{j\uparrow} \\ \hat{a}_{j\downarrow} \end{pmatrix}, \quad j = 1, 2, 3, \quad (\text{A1})$$

where the unitary operators  $\hat{U}_j = \cos \frac{\theta_j}{2} \hat{1} - i \sin \frac{\theta_j}{2} \mathbf{n} \hat{\sigma}$  represent rotation through the angles  $\theta_1 = 0$ ,  $\theta_2 = 2\pi/3$ ,  $\theta_3 = 4\pi/3$ .

For further simplification we take the permutation symmetry of the magnetic sublattices<sup>24</sup> into account and introduce the following combinations of operators  $\hat{b}_{j\tau}$

$$\begin{aligned} \hat{\xi}_{1\tau} &= \frac{1}{\sqrt{6}} (2\hat{b}_{1\tau} - \hat{b}_{2\tau} - \hat{b}_{3\tau}), \hat{\xi}_{2\tau} = \frac{1}{\sqrt{2}} (\hat{b}_{2\tau} - \hat{b}_{3\tau}), \\ \hat{\xi}_{3\tau} &= \frac{1}{\sqrt{3}} (\hat{b}_{1\tau} + \hat{b}_{2\tau} + \hat{b}_{3\tau}) \end{aligned} \quad (\text{A2})$$

that form irreducible representations of permutation group  $P_3$  (isomorphic to  $C_3$  rotation group which describes the exchange symmetry of the compound).

Operators  $\{\hat{b}_{j\tau}, \hat{b}_{j\tau}^\dagger\}$  and  $\{\hat{\xi}_{j\tau}, \hat{\xi}_{j\tau}^\dagger\}$  satisfy the same anticommutation relations as Fermi operators  $\{\hat{a}_{j\tau}, \hat{a}_{j\tau}^\dagger\}$ .

It is worth to mention that the operators  $\{\hat{\xi}_{1\tau}, \hat{\xi}_{2\tau}\}$  belong to the same irreducible representation as the AFM vectors  $\{\mathbf{L}_1, \mathbf{L}_2\}$ , and operator  $\{\hat{\xi}_{3\tau}\}$  has the same transformation properties as magnetization vector  $\mathbf{M}$  (see equation (2)).

As it was already mentioned, in the AFM ground state  $\mathbf{M} = \mathbf{0}$ ,  $\mathbf{L}_1 \perp \mathbf{L}_2 \perp \mathbf{n}$ ,  $|\mathbf{L}_1| = |\mathbf{L}_2| = S$ .<sup>24</sup> We take the quantization axis for free spins parallel to  $\mathbf{L}_1$ .

Taking account of transformations (A1), (A2) the hamiltonian (6) takes a form

$$\begin{aligned} \hat{H}(\mathbf{r}, t) &= -J_{sd} S \sum_j \left( \hat{\xi}_{j\uparrow}^\dagger \hat{\xi}_{j\uparrow} - \hat{\xi}_{j\downarrow}^\dagger \hat{\xi}_{j\downarrow} \right) + \gamma(\mathbf{k}) \left[ 2\hat{\xi}_{3\tau}^\dagger \hat{\xi}_{3\tau} - \left( \hat{\xi}_{1\tau}^\dagger \hat{\xi}_{1\tau} + \hat{\xi}_{2\tau}^\dagger \hat{\xi}_{2\tau} \right) \right. \\ &\quad \left. + 3 \left( \hat{\xi}_{1\downarrow}^\dagger \hat{\xi}_{2\uparrow} + \hat{\xi}_{2\uparrow}^\dagger \hat{\xi}_{1\downarrow} - \hat{\xi}_{2\downarrow}^\dagger \hat{\xi}_{1\uparrow} - \hat{\xi}_{1\uparrow}^\dagger \hat{\xi}_{2\downarrow} \right) \right], \end{aligned} \quad (\text{A3})$$

which now can be easily diagonalized.

## Appendix B: Berry connection, Berry curvature and dynamics equations

To simplify the calculation of the Berry connection (19) we note that i) time/space dependence of the state vectors  $|\Psi_{2a}(r_\mu)\rangle$ ,  $|\Psi_{2b}(r_\mu)\rangle$  stems from the rotation of the spin



quantization axis; ii) rotation of the local frame (unit vectors  $\mathbf{e}_k(r_\mu)$ ,  $k = x, y, z$ ) can be equivalently represented in terms of the rotation matrix  $\mathfrak{R}$  (3):  $\mathbf{e}_k(r_\mu) \equiv \mathfrak{R}(\boldsymbol{\varphi})\mathbf{e}_k^0$  or related unitary matrix  $\hat{U}$  (14):  $\mathbf{e} \hat{\boldsymbol{\sigma}} = \hat{U}\mathbf{e}^0\hat{\boldsymbol{\sigma}}\hat{U}^\dagger$ , where  $\mathbf{e}_k^0$  is taken at some reference point  $r_\mu^0$ . The same matrix  $\hat{U}$  defines transformation (15) of state the vectors  $|\Psi_2(r_\mu)\rangle$ . An analogous procedure was proposed in Ref. 54. So, the Berry connection  $\hat{\mathcal{A}}_\mu^r$  can be expressed as

$$\hat{\mathcal{A}}_\mu^r = i \begin{pmatrix} \langle \Psi_{2a}^0 | \hat{\Lambda}_\mu \Psi_{2a}^0 \rangle & \langle \Psi_{2a}^0 | \hat{\Lambda}_\mu \Psi_{2b}^0 \rangle \\ \langle \Psi_{2b}^0 | \hat{\Lambda}_\mu \Psi_{2a}^0 \rangle & \langle \Psi_{2b}^0 | \hat{\Lambda}_\mu \Psi_{2b}^0 \rangle \end{pmatrix}, \quad (\text{B1})$$

where we introduced the matrix  $\hat{\Lambda}_\mu \equiv \hat{U}^\dagger \partial_\mu^r \hat{U}$ . Direct calculations show that

$$\hat{\Lambda}_\mu = -\frac{i}{2} \mathfrak{R}^{-1}(\boldsymbol{\varphi}) \boldsymbol{\Omega}_\mu \hat{\boldsymbol{\sigma}}. \quad (\text{B2})$$

and

$$\hat{\mathcal{A}}_\mu^r = \left( \frac{1}{2} \sin 2\psi \mathfrak{R}^{-1}(\boldsymbol{\varphi}) \boldsymbol{\Omega}_\mu + \frac{1}{4} (1 - \sin 2\psi) \mathbf{n}_0 \times \mathfrak{R}^{-1}(\boldsymbol{\varphi}) \boldsymbol{\Omega}_\mu \times \mathbf{n}_0 \right) \hat{\boldsymbol{\sigma}}. \quad (\text{B3})$$

From (B3) after some simple math one gets expr. (21).

It is obvious from relations (B1), (B2) that the singlet states with zero spin do not contribute to the Berry connection.

The spin vector  $\mathbf{s}(t, \mathbf{r}) = \langle w | \hat{\boldsymbol{\sigma}} | w \rangle$  is calculated in a similar way with the help of matrix  $\hat{\Sigma} \equiv \hat{U}^\dagger \hat{\boldsymbol{\sigma}} \hat{U} = \mathfrak{R}(\boldsymbol{\varphi}) \mathbf{e}_k^0 \hat{\boldsymbol{\sigma}}_k$ , explicit relation being

$$\mathbf{s}(t, \mathbf{r}) = \mathfrak{R}(\boldsymbol{\varphi}) \left[ \sin 2\psi \mathbf{C} + \frac{1}{2} (1 - \sin 2\psi) \mathbf{n}_0 \times (\mathbf{C} \times \mathbf{n}_0) \right]. \quad (\text{B4})$$

Using the relation  $\mathbf{n} = \mathfrak{R}(\boldsymbol{\varphi}) \mathbf{n}_0$  between the vectors in the local and reference frame one gets expression (29) from (B4).

Equation (B4) is easily inverted in order to express the isospin  $\mathbf{C}$  through the real spin as follows:

$$\mathbf{C} = \frac{2}{1 + \sin 2\psi} \mathfrak{R}^{-1}(\boldsymbol{\varphi}) \left[ \mathbf{s}(t, \mathbf{r}) + \frac{1 - \sin 2\psi}{2 \sin 2\psi} (\mathbf{n} \mathbf{s}) \mathbf{n} \right] \quad (\text{B5})$$

Substituting relation (B5) into the normalization condition  $|\mathbf{C}|^2 = 1$  one gets equation (30) for spheroid.

The Berry curvatures (22) are calculated by differentiation of (B3) with account of two general relations:

$$\dot{\mathfrak{R}}(\boldsymbol{\varphi}) = \boldsymbol{\Omega} \times \mathfrak{R}(\boldsymbol{\varphi}) \quad \text{and} \quad \partial_\nu^r \boldsymbol{\Omega}_\mu - \partial_\mu^r \boldsymbol{\Omega}_\nu = \boldsymbol{\Omega}_\mu \times \boldsymbol{\Omega}_\nu. \quad (\text{B6})$$

Dynamic equation (31) for the spin is obtained by differentiation of the expression (29) with the use of relations (B6), (16) and (B5).

The complete equation for acceleration has the following form:

$$\dot{k}_\mu = -\partial_\mu^r \varepsilon_2 - \frac{1}{2} \dot{\mathbf{s}} \cdot \boldsymbol{\Omega}_\mu - \frac{1}{2} \dot{k}_\nu \partial_\nu^k \ln(1 + \sin 2\psi) \left[ \mathbf{s} \cdot \boldsymbol{\Omega}_\mu + \frac{1}{\sin 2\psi} (\mathbf{ns}) (\mathbf{n}\boldsymbol{\Omega}_\mu) \right]. \quad (\text{B7})$$

- 
- <sup>1</sup> X. Tang, H.-W. Zhang, H. Sua, Y.-L. Jing, and Z.-Y. Zhong, *J. Magn. Mag. Mater.* **321**, 1851 (2009).
- <sup>2</sup> T. Kampfrath, A. Sell, G. Klatt, A. Pashkin, S. Mahrlein, T. Dekorsy, M. Wolf, M. Fiebig, A. Leitenstorfer, and R. Huber, *Nat Photon* **5**, 31 (2011).
- <sup>3</sup> P. Haney, R. Duine, A. S. Nunez, and A. MacDonald, *J. Magn. Magn. Mater.* **320**, 1300 (2008).
- <sup>4</sup> H. Gomony and V. Loktev, *J. Magn. Soc. .Japan* **32**, 535 (2008).
- <sup>5</sup> E. V. Gomony and V. M. Loktev, *Low Temperature Physics* **34**, 198 (2008).
- <sup>6</sup> R. Cheng, J. Xiao, Q. Niu, and A. Brataas, *Phys. Rev. Lett.* **113**, 057601 (2014).
- <sup>7</sup> K. M. D. Hals, Y. Tserkovnyak, and A. Brataas, *Phys. Rev. Lett.* **106**, 107206 (2011).
- <sup>8</sup> E. G. Tveten, A. Qaiumzadeh, O. A. Tretiakov, and A. Brataas, *Phys. Rev. Lett.* **110**, 127208 (2013).
- <sup>9</sup> J. Železný, H. Gao, K. Výborný, J. Zemen, J. Mašek, A. Manchon, J. Wunderlich, J. Sinova, and T. Jungwirth, *Phys. Rev. Lett.* **113**, 157201 (2014).
- <sup>10</sup> H. Chen, Q. Niu, and A. MacDonald, *Phys. Rev. Lett.* **112**, 017205 (2014).
- <sup>11</sup> J. Kübler and C. Felser, *ArXiv e-prints* (2014), arXiv:1410.5985.
- <sup>12</sup> P. Bruno, V. K. Dugaev, and M. Taillefumier, *Phys. Rev. Lett.* **93**, 096806 (2004).
- <sup>13</sup> N. Nagaosa, J. Sinova, S. Onoda, A. H. MacDonald, and N. P. Ong, *Rev. Mod. Phys.* **82**, 1539 (2010).
- <sup>14</sup> H. Takatsu, S. Yonezawa, S. Fujimoto, and Y. Maeno, *Phys. Rev. Lett.* **105**, 137201 (2010).
- <sup>15</sup> C. Sürgers, G. Fischer, P. Winkel, and H. v. Löhneysen, *Nature Comm.* **5**, 3400 (2014).
- <sup>16</sup> Y. Tserkovnyak and C. H. Wong, *Phys. Rev. B* **79**, 014402 (2009).
- <sup>17</sup> R. Cheng and Q. Niu, *Phys. Rev. B* **86**, 245118 (2012).
- <sup>18</sup> S. E. Barnes and S. Maekawa, *Phys. Rev. Lett.* **98**, 246601 (2007).
- <sup>19</sup> F. Freimuth, R. Bamler, Y. Mokrousov, and A. Rosch, *Phys. Rev. B* **88**, 214409 (2013).

- <sup>20</sup> E. Bertaut, D. Fruchart, J. Bouchaud, and R. Fruchart, *Solid State Comm.* **6**, 251 (1968).
- <sup>21</sup> J.P. Jardin and J. Labbé, *J. Phys. France* **36**, 1317 (1975).
- <sup>22</sup> Z. Ali, M. Shafiq, S. J. Asadabadi, H. R. Aliabad, I. Khan, and I. Ahmad, *Computational Materials Science* **81**, 141 (2014).
- <sup>23</sup> K. Motizuki and H. Nagai, *J. Phys. C* **21**, 5251 (1988).
- <sup>24</sup> E. V. Gomonaj and V. A. L'vov, *Phase Transitions* **38**, 15 (1992).
- <sup>25</sup> E. V. Gomonaj and V. A. L'vov, *Phase Transitions* **40**, 225 (1992).
- <sup>26</sup> P. Lukashev and R. F. Sabirianov, *Phys. Rev. B* **82**, 094417 (2010).
- <sup>27</sup> E. Chi, W. Kim, and N. Hur, *Solid State Comm.* **120**, 307 (2001).
- <sup>28</sup> K. Takenaka, A. Ozawa, T. Shibayama, N. Kaneko, T. Oe, and C. Urano, *Appl. Phys. Lett.* **98**, 022103 (2011).
- <sup>29</sup> Strictly speaking,  $\Gamma^{4g}$  structure realized in a certain temperature range is consistent with weak ferromagnetic structure in which vectors  $\mathbf{S}_j$  slightly deviate from the plane. We, however, neglect small noncompensated magnetization for the sake of simplicity.
- <sup>30</sup> A. F. Andreev and V. I. Marchenko, *Physics-Uspekhi* **23**, 21 (1980).
- <sup>31</sup> H. V. Gomonay, R. V. Kunitsyn, and V. M. Loktev, *Phys. Rev. B* **85**, 134446 (2012).
- <sup>32</sup> L. Chu, C. Wang, J. Yan, Y. Na, L. Ding, Y. Sun, and Y. Wen, *Scripta Mater.* **67**, 173 (2012).
- <sup>33</sup> G. Sundaram and Q. Niu, *Phys. Rev. B* **59**, 14915 (1999).
- <sup>34</sup> D. Xiao, M.-C. Chang, and Q. Niu, *Rev. Mod. Phys.* **82**, 1959 (2010).
- <sup>35</sup> D. Culcer, Y. Yao, and Q. Niu, *Phys. Rev. B* **72**, 085110 (2005).
- <sup>36</sup> Note, that we discuss only rotations in spin state, the lattice itself is supposed to be unchanged. However, the theory can be generalized to include space rotations of lattice, as will be discussed below. See also Ref.33 for description of gauge fields in the deformed crystals.
- <sup>37</sup> Y. Tserkovnyak and M. Mecklenburg, *Phys. Rev. B* **77**, 134407 (2008).
- <sup>38</sup> N. Nagaosa and Y. Tokura, *Nat Nano* **8**, 899 (2013).
- <sup>39</sup> G. E. Volovik, *J. Phys. C* **20**, L83 (1987).
- <sup>40</sup> A.M.Kosevich, B.A.Ivanov, and A.S.Kovalev, *Nonlinear magnetization waves. Dynamical and topological solitons* (Naukova Dumka, Kiev, 1983) 189 p.(in Russian).
- <sup>41</sup> R. Rajaraman, *Solitons And Instantons: An Introduction To Solitons And Instantons In Quantum Field Theory* (North-Holland, Amsterdam).
- <sup>42</sup> Y. B. Bazaliy, B. A. Jones, and S.-C. Zhang, *Phys. Rev. B* **57**, R3213 (1998).

- <sup>43</sup> Strictly speaking, an effective charge should be introduced as a vector quantity, so, for the sake of simplicity we introduce combination of charge and fields. However, Faraday's relation for fields  $\varepsilon_{\xi\mu\nu}\partial_\mu E_\nu + \partial_t B_\xi = 0$  is satisfied.
- <sup>44</sup> R. Shindou and N. Nagaosa, Phys. Rev. Lett. **87**, 116801 (2001).
- <sup>45</sup> Formally, it is combination  $q\mathbf{B}$  that has pseudo-vector character, due to the dependence on pseudovector  $\mathbf{s}$  (see (37)). So, in our case time-inversion symmetry is broken rather by the effective charge than by the effective field.
- <sup>46</sup> X. Martí, B. G. Park, J. Wunderlich, H. Reichlová, Y. Kurosaki, M. Yamada, H. Yamamoto, A. Nishide, J. Hayakawa, H. Takahashi, and T. Jungwirth, Phys. Rev. Lett. **108**, 017201 (2012).
- <sup>47</sup> The proposed model distribution of AFM order parameter has a peculiarity at  $r \rightarrow 0$  which can be avoided by placing a defect or a hole in the center.
- <sup>48</sup> Spin rotation which arises during the passage through the domain wall, can reduce the deflection. However, due to  $1/r$  dependency of the Lorentz force the effect can be still pronounced close to the center of the region.
- <sup>49</sup> J. Lin, B. Wang, P. Tong, S. Lin, W. Lu, X. Zhu, Z. Yang, W. Song, J. Dai, and Y. Sun, Scripta Materialia **65**, 452 (2011).
- <sup>50</sup> L. Szunyogh, B. Lazarovits, L. Udvardi, J. Jackson, and U. Nowak, Phys. Rev. B **79**, 020403(R) (2009).
- <sup>51</sup> A. Kohn, A. Kovacs, R. Fan, G. J. McIntyre, R. C. C. Ward, and J. P. Goff, Sci. Rep. (2013).
- <sup>52</sup> I. Raičević, D. Popović, C. Panagopoulos, L. Benfatto, M. B. Silva Neto, E. S. Choi, and T. Sasagawa, Phys. Rev. Lett. **106**, 227206 (2011).
- <sup>53</sup> K. Kim, M.-S. Chang, S. Korenblit, R. Islam, E. E. Edwards, G.-D. Freericks, J. K. and Lin, L.-M. Duan, and C. Monroe, Nature **465**, 590 (2010).
- <sup>54</sup> G. Tatara and H. Fukuyama, Phys. Rev. Lett. **78**, 3773 (1997).